LABORATORY STUDIES ON THE FORMATION OF OZONE (O₃) ON ICY SATELLITES AND ON INTERSTELLAR AND COMETARY ICES

CHRIS J. BENNETT[1] AND RALF I. KAISER[1,2,3]

ABSTRACT

The formation of ozone (O₃) in neat oxygen ices was investigated experimentally in a surface-scattering machine. At 11 K, solid oxygen was irradiated with energetic electrons; the chemical modification of the target was followed on-line and in situ via Fourier transform infrared spectroscopy (FTIR; solid state) and quadrupole mass spectrometry (QMS; gas phase). The dominant product identified was the ozone molecule in the bent, C_{2v} symmetric structure, $O_3(X\,^1A_1)$; the cyclic D_{3h} isomer was not observed. The associated van der Waals complexes [O₃ . . . O] and [O₃ . . . O₃] could also be detected via infrared spectroscopy, verifying explicitly the existence of oxygen atoms in the matrix at 11 K. Three different formation mechanisms of ozone were revealed. Two pathways involve the reaction of suprathermal oxygen atoms with molecular oxygen $[O_2(X\,^3\Sigma_g^-)]$ at 11 K. Once the sample was warmed after the irradiation to about 38 K, a third, thermal reaction pathway involving the barrierless reaction of ground-state oxygen atoms with molecular oxygen sets in. During the warm-up phase, the inherent sublimation of oxygen and ozone was monitored by mass spectrometry and occurs in the ranges 28–43 and 58–73 K, respectively. Our data are of help to understand the mechanisms of ozone formation within apolar interstellar and cometary ices and could also be applicable to outer solar system icy bodies, such as the moons of Jupiter (Ganymede, Europa, and Callisto) and Saturn (Rhea and Dione), where ozone and/or condensed oxygen has been observed.

Subject headings: astrochemistry — cosmic rays — ISM: molecules — methods: laboratory — molecular processes — planets and satellites: general

1. INTRODUCTION

The importance of the ozone layer in Earth's atmosphere was realized in 1881 by Hartley (1881)—ozone (O₃), during photodissociation, absorbs ultraviolet (UV) light strongly between 200 and 320 nm ($\lambda_{max} = 254$ nm), which is extremely damaging to life, particularly to DNA ($\lambda_{max} = 260$ nm; Okabe 1978; Thomas 1993). Ozone is produced within the terrestrial atmosphere in the gas phase by the following reaction scheme, similar to the one originally proposed in 1930 by Chapman (1930):

$$O_2(X\,^3\Sigma_g^-) + h\nu\,(<240\text{ nm}) \rightarrow O(^3P) + O(^3P), \quad (1)$$

$$O_2(X\,^3\Sigma_g^-) + O(^3P) + M \rightarrow O_3(X\,^1A_1) + M^*. \quad (2)$$
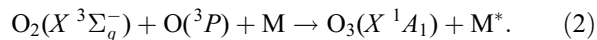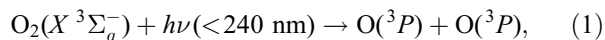
Reaction (1) requires light of a wavelength below 240 nm, implying that the energy required to break the bond in molecular oxygen is 498 kJ mol⁻¹ (5.17 eV); thus, the heat of formation ($\Delta_f H^\circ$) for a single oxygen atom in its ground state is 249 kJ mol⁻¹ (2.58 eV). Since the production of ozone via equation (2) is exothermic ($\Delta_f H^\circ = -143$ kJ mol⁻¹, −1.48 eV), the presence of a third body, M (N₂ or O₂ in our atmosphere), is crucial in order to carry away some of the excess energy (107 kJ mol⁻¹, 1.10 eV) to stabilize the internally excited ozone molecule formed via reaction (2).[4]

Owen (1980) suggested that a planet that harbors life should be rich in oxygen (O₂) and water. The detection of chemical species on an extrasolar planet using visible and radio frequencies is problematic (Léger 2000); thus, use of the mid-infrared region to detect molecular vibrations is the most promising. However, the selection rules dictate that a vibration must change the molecular dipole moment to be infrared active. Since molecular oxygen has no dipole moment and is symmetric, the fundamental vibration is infrared forbidden. On the other hand, the ozone abundance is fairly insensitive to the oxygen concentration and is expected to be a logarithmic tracer for oxygen in planetary atmospheres (Angel et al. 1986; Kasting & Catling 2003). Coupled with its UV-shielding properties, it is hardly surprising that detection of the strongly infrared active 9.6 μm (1041 cm⁻¹) band of ozone has been selected as one of the primary goals of both the *Terrestrial Planet Finder* (*TPF*; NASA) and *Darwin* (ESA) interferometer space telescopes (Beichman et al. 1999; Léger 2000). However, to be certain that molecular oxygen and hence ozone is really based on active life on an extraterrestrial planet, it has been recognized that we must also understand possible abiotic production processes of oxygen/ozone observed within our solar system to rule out the possibility of "false positive detections" (Selsis et al. 2002). For example, although ozone has been detected on Mars (Barth et al. 1973), there is not much evidence to support that it has a biogenic origin.

Astrochemical models of dark clouds predict that condensed oxygen is likely to be a major component of apolar dust grains within interstellar clouds ($T \sim 10$ K), which will be chemically processed by irradiation from Galactic cosmic-ray particles (predominantly MeV–GeV protons) and the internal UV field (Tielens & Hagen 1982; Mathis et al. 1983; Greenberg 1984; Strazzulla & Johnson 1991). There is also some evidence of condensed oxygen on the icy satellites of Jupiter and Saturn; the 5773 Å visible absorption band arising from interacting pairs of O₂ molecules has been detected on Ganymede (Spencer et al. 1995) and, more recently, on Europa and Callisto (Spencer &

[1] Department of Chemistry, University of Hawai'i at Manoa, Honolulu, HI 96822.

[2] Department of Physics and Astronomy, The Open University, Milton Keynes MK7 6AA, UK.

[3] Corresponding author: kaiser@gold.chem.hawaii.edu.

[4] Values taken from http://webbook.nist.gov/chemistry.
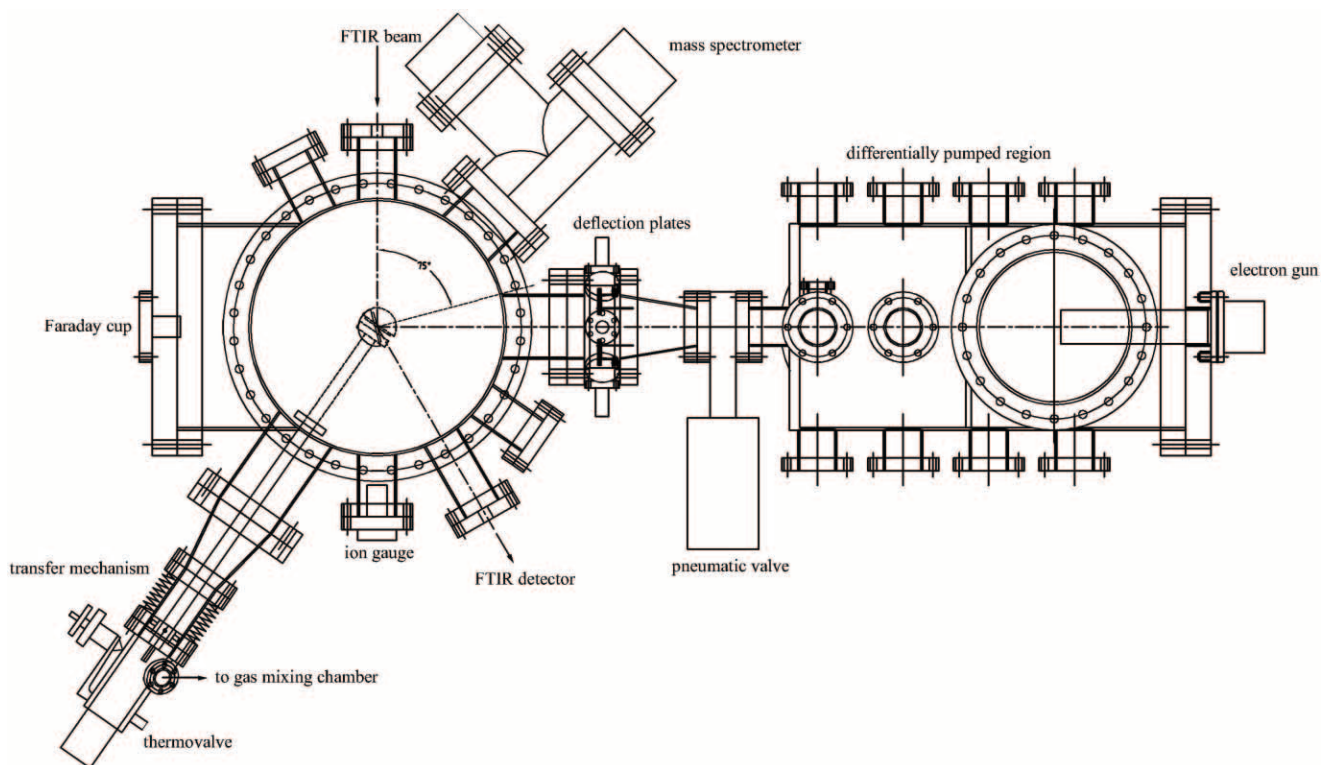
FIG. 1.—Top view of the experimental setup.

Calvin 2002). There is some debate as to whether or not condensed oxygen would be stable for long periods at the temperatures of these bodies (90–150 K). This led to the proposal of bubbles of oxygen formed in ion tracks (Johnson & Jesser 1997); likewise, the signal could emanate from cooler icy patches, where oxygen may be stable (Calvin & Spencer 1997), or from an atmospheric haze (Vidal et al. 1997). Evidence for chemical processing comes from the detection of atomic oxygen in the UV airglows of Europa and Ganymede from the 1304 and 1356 Å emission lines (Hall et al. 1998); in addition, the detection of ozone via its UV absorption at 260 nm on Ganymede (Noll et al. 1996) as well as on two icy satellites of Saturn, Rhea and Dione (Noll et al. 1997), is confirmed. These icy satellites are continually bombarded by energetic particles from the magnetospheres of Jupiter and Saturn, with the highest energy flux coming from an energetic electron bombardment (Cooper et al. 2001).

The use of energetic electrons to bombard our solid oxygen sample is twofold. First, we study the effects of energetic electrons of the planetary magnetospheres interacting with oxygen ices. Second, we have the additional benefits of simulating the energetic electrons released via primary ionization processes in the track of the Galactic cosmic-ray particles in interstellar and cometary ices (Oort cloud). Most importantly, the averaged linear energy transfer (LET) of keV electrons is comparable to that of MeV protons (typically a few keV per μm); therefore, we can also simulate the inelastic energy transfer processes occurring without the need for a cyclotron (Johnson 1990). This paper is the first in a series of a systematic research program that aims to investigate the formation of ozone using varied energetic particles (electrons, protons, and photons), target compositions (neat oxygen and binary mixtures with water), and temperatures (10 K, relevant to molecular clouds and comets in the Oort cloud, to 150 K, relevant to the Jovian satellites). Previous studies on condensed oxygen include energetic processing by

UV photons (Crowley & Sodeau 1989; Schriver-Mazzuoli et al. 1995; Gerakines et al. 1996; Dyer et al. 1997), keV protons (Baragiola et al. 1999; Fama et al. 2002), and electrons (Lacombe et al. 1997 and references therein) and will be discussed in this context.

2. EXPERIMENTAL

The experimental setup is shown in Figure 1. Briefly, an ultrahigh vacuum (UHV) chamber is evacuated down to a base pressure of typically 5×10^{-11} torr using oil-free magnetically suspended turbomolecular pumps. In the center of the chamber is a rotatable highly polished silver monocrystal, which is cooled to 11.0 ± 0.3 K by a closed-cycle helium refrigerator. The molecular oxygen (O_2) frost was prepared by depositing oxygen (99.998%) for 5 minutes at a pressure of 10^{-7} torr onto the cooled silver crystal. The condensed sample is inspected via a Nicolet 510 DX Fourier transform infrared spectrometer (242 scans over 5 minutes from 6000 to 400 cm^{-1} with a resolution of 2 cm^{-1}) operating in absorption-reflection-absorption mode (reflection angle $\alpha = 75°$). The gas phase is monitored by a quadrupole mass spectrometer (Balzer QMG 420) operating in residual gas analyzer mode with the electron impact ionization energy at 90 eV.

The samples were then irradiated isothermally at 11.0 ± 0.3 K with 5 keV electrons generated with an electron gun (Specs EQ 22/35) at beam currents of 100 nA for 50 minutes by scanning the electron beam over an area of 3.0 ± 0.4 cm^2. In theory, this would mean that during the irradiation the sample would be exposed to a total of 1.9×10^{15} electrons (6.2×10^{14} electrons cm^{-2}); however, not all of the electrons generated by our electron gun actually reach the target—the manufacturer states an extraction efficiency of 78.8%, meaning that the actual number of electrons that hit the sample is reduced to 1.5×10^{15} electrons (4.9×10^{14} electrons cm^{-2}). After the irradiation is complete, the
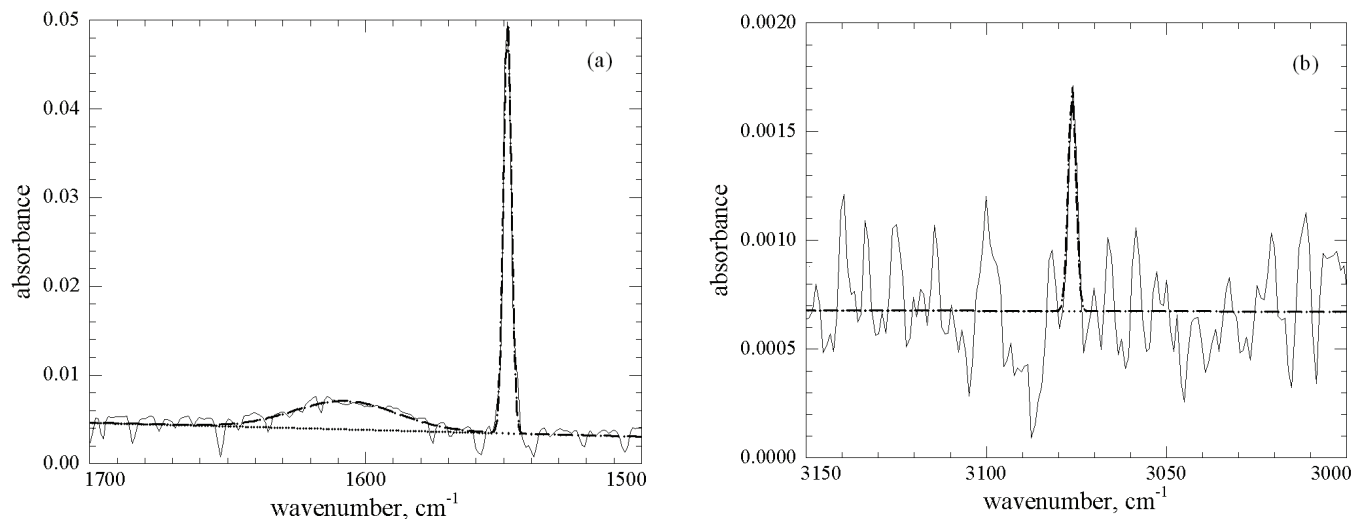
Fig. 2.—Infrared spectrum of the oxygen frost at 11 K. The fundamental and the lattice modes are shown in (a), and the first overtone of the fundamental is shown in (b). The dot-dashed lines represent Gaussian fits to each peak. The assignments are compiled in Table 1.

sample is then left isothermally for 1 hr before it is heated at a rate of 0.5 K minute^{-1}.

Figure 2 depicts a typical infrared spectrum of the condensed oxygen frost prior to the irradiation; the absorptions are compiled in Table 1. In general, the column density N (molecules cm^{-2}) can be calculated via a modified Lambert-Beer relationship (see Bennett et al. 2004 for more details),

$$N = \frac{\ln 10}{2} \cos \alpha \frac{\int_{\nu_1}^{\nu_2} A(\nu) \, d\nu}{A}, \qquad (3)$$

where the division by a factor of 2 corrects for the ingoing and outgoing infrared beam, α is the angle between the normal of the surface mirror and the infrared beam, $\int_{\nu_1}^{\nu_2} A(\nu) \, d\nu$ is the integrated area of the infrared absorption feature for our sample (cm^{-1}), and A is the integrated absorption coefficient (cm molecule^{-1}). However, this process is complicated by the fact that in case of molecular oxygen, there are large variations in the integrated absorption coefficients of an intrinsic infrared-inactive band in the gas phase. Using a value of 3.8×10^{-22} cm for A for the fundamental extrapolated from Cairns & Pimentel (1965) and a density of 1.54 g cm^{-3} (Freiman & Jodl 2004), we would determine our ice thickness to be 46 μm. On the other hand, using values estimated by Ehrenfreund et al. (1992) at $A = 1 \times 10^{-19}$ cm, our thickness would be only 0.2 μm. Using a more recent value of $A = 5 \times 10^{-21}$ cm gives an ice thickness of 3.5 μm (Vandenbussche et al. 1999). In pure crystalline α-O$_2$, however, the symmetry of the crystal structure forbids the fundamental from being infrared active; only lattice modes can be observed (Freiman & Jodl 2004). The only reason the fundamental is visible in our spectra and also that of Cairns &

Pimentel (1965) is that crystal imperfections reduce the symmetry of the crystal structure; as a consequence, an electric dipole moment is induced. The ratio of the fundamental (1549 cm^{-1}) to the libration band (1614 cm^{-1}) in our sample is about 1, compared to values ranging from 1:2 to 1:20 as found by Cairns & Pimentel (1965). This indicates that our oxygen exists primarily in an amorphous phase. An alternative interpretation is given by Jones et al. (1986), where the authors state the formation of a metastable amorphous phase, which exists between 8 and 12 K (Jones et al. 1985, 1986). Based on these considerations, the sample thickness in our experiments is likely to be in the lower micron range.

3. RESULTS

3.1. Infrared Spectroscopy

The only new molecule synthesized as a result of the irradiation is the bent C_{2v} structure of ozone; the cyclic D_{3h} isomer was not observed (Siebert & Schinke 2003). We observe the ozone molecule, O$_3(X\,^1A_1)$, via eight absorption bands: the three fundamentals ν_1, ν_2, and ν_3 appear at 1104, 702, and 1037 cm^{-1}, respectively (Fig. 3), whereas the overtones $2\nu_3$ and $3\nu_3$ were found at 2044 and 3028 cm^{-1}; the combination bands $\nu_1 + \nu_3$, $\nu_2 + \nu_3$, and $\nu_1 + \nu_2 + \nu_3$ could be detected at 2105, 1721, and 2798 cm^{-1}, respectively. The positions of these absorptions agree well with previous studies (Brewer & Wang 1972; Gerakines et al. 1996; Schriver-Mazzuoli et al. 1995; Dyer et al. 1997; Chaabouni et al. 2000). The band positions and their assignments are listed in Table 2 along with integrated absorption coefficients calculated by Adler-Golden et al. (1985); the latter help to explain the relative intensities of the peaks, in particular the weak combination band $\nu_1 + \nu_2 + \nu_3$, which is only visible during warm-up, when the column density of the ozone almost doubles (see below).

To extract mechanistic studies on the formation of ozone, we have to investigate the fine structure of the bands closer. Upon the onset of the irradiation, the ν_3 fundamental immediately separates into two peaks (Fig. 3c), one relating to the matrix-isolated ozone monomer observed at 1037 cm^{-1} and a second associated with the formation of an [O$_3$...O] van der Waals complex at 1032 cm^{-1} (Schriver-Mazzuoli et al. 1995; Dyer et al. 1997). During the early stages of irradiation, the absorption band

TABLE 1

Infrared Absorptions of the Oxygen Frost and Assignment of the Observed Bands According to Freiman & Jodl (2004)

Frequency (cm^{-1})	Assignment	Characterization
1549	ν_1	O-O stretching (fundamental)
1614	$\nu_1 + \nu_L$	Fundamental + lattice mode
3076	$2\nu_1$	Overtone of fundamental
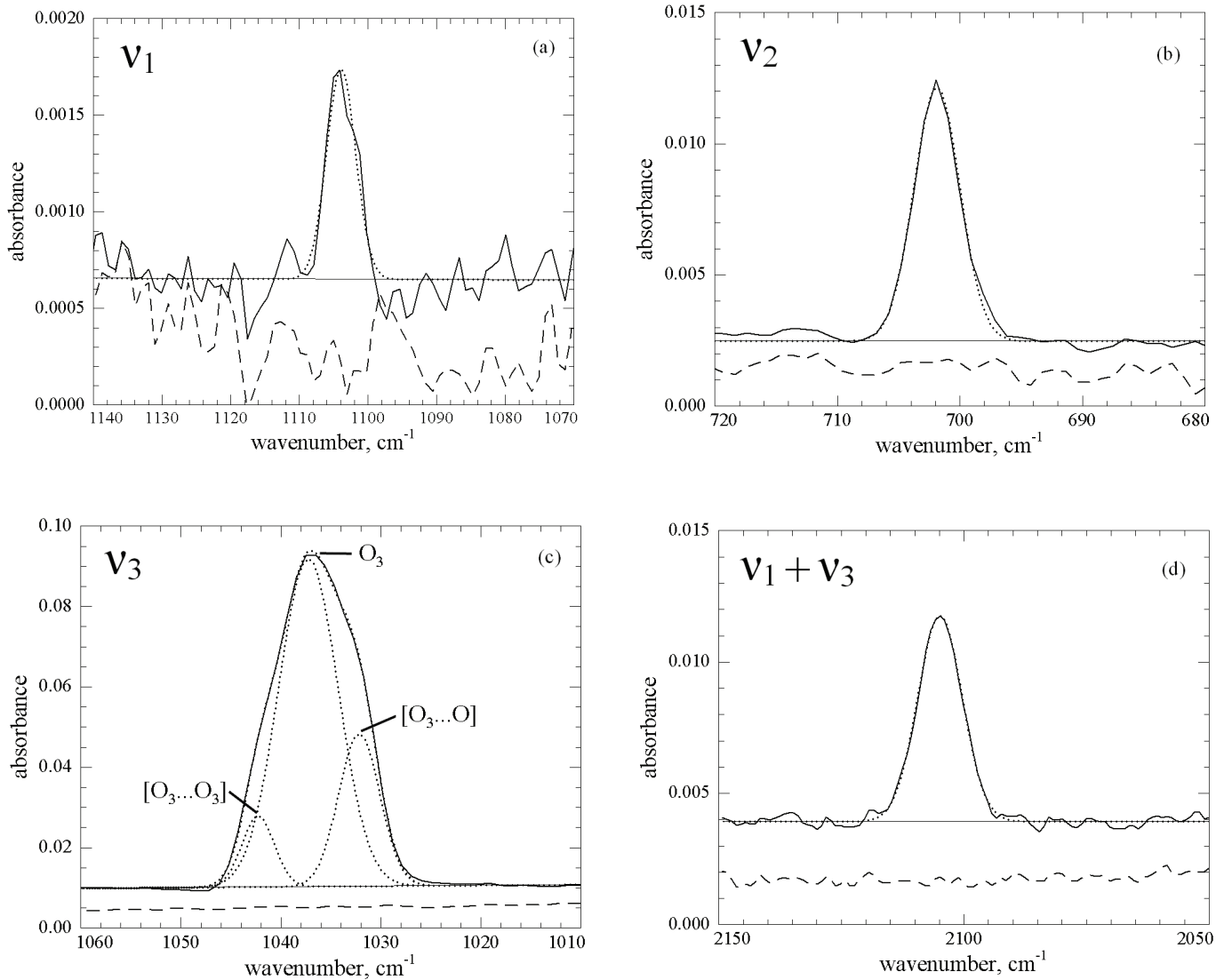
FIG. 3.—Infrared absorptions from the formation of ozone as seen before (*dashed lines*) and after (*solid lines*, with Gaussian fits as dotted lines) the irradiation of the oxygen sample at 11 K with a beam current of 100 nA: (*a*) ν_1, (*b*) ν_2, (*c*) ν_3, and (*d*) $\nu_1 + \nu_3$. The complete list of observed bands and assignments is given in Table 2.

TABLE 2

OBSERVED PEAKS AFTER IRRADIATION AND CALCULATED INTEGRATED ABSORPTION COEFFICIENTS

Frequency (cm^{-1})	Assignment	Characterization	A (cm molecule^{-1})
1104.....................................	O_3 (ν_1)	O-O symmetric stretch	1.84×10^{-19}
702.....................................	O_3 (ν_2)	O-O-O bend	7.11×10^{-19}
1037.....................................	O_3 (ν_3)	O-O asymmetric stretch	1.53×10^{-17}
2044.....................................	O_3 ($2\nu_3$)	Overtone	5.80×10^{-20}
3028.....................................	O_3 ($3\nu_3$)	Overtone	1.23×10^{-19}
1721.....................................	O_3 ($\nu_2 + \nu_3$)	Combination band	6.01×10^{-20}
2105.....................................	O_3 ($\nu_1 + \nu_3$)	Combination band	1.30×10^{-18}
2798[a].....................................	O_3 ($\nu_1 + \nu_2 + \nu_3$)	Combination band	3.31×10^{-20}

NOTES.—Irradiation was for 50 minutes via 5 keV electrons at 100 nA. Values for the integrated absorption coefficients were taken from Adler-Golden et al. (1985). Assignments of the observed bands are according to Brewer & Wang (1972).

[a] Only visible during the warm-up period at 35 K.
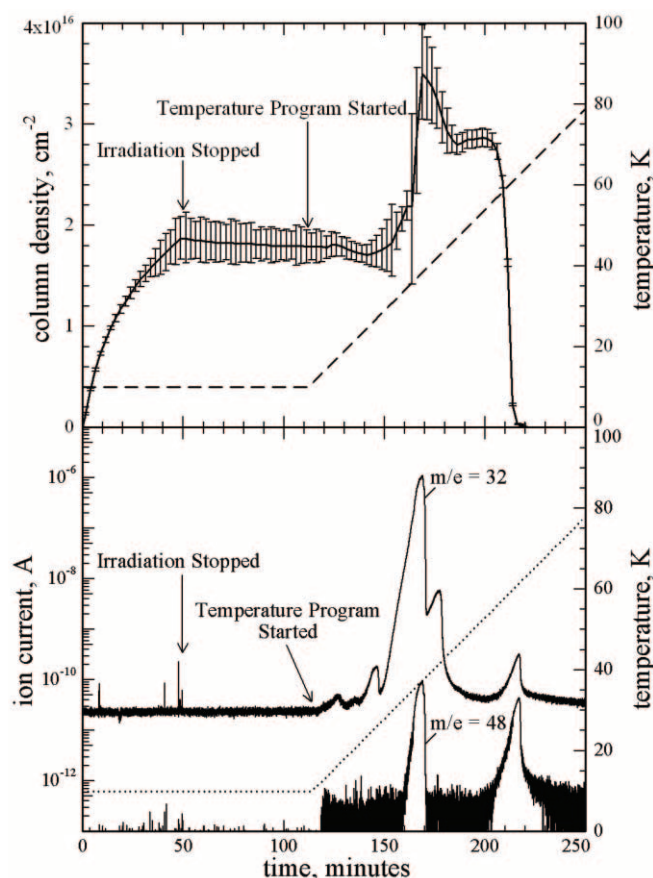
FIG. 4.—Temporal profile of the column density of ozone calculated via the integrated absorption at 1037 cm^{-1} (*top*) and mass spectrometric signals at $m/e = 32$ and 48 (*bottom*) during the irradiation, isothermal phase, and heating period. The corresponding temperature profile is overlaid.

FIG. 5.—Temporal development of the ozone partial pressure as extracted from the raw data (mass spectrometry) via matrix interval algebra; the error bars of about 30% have been removed for clarity. The corresponding temperature profile is overlaid.

of the [$O_3 \ldots O$] complex is of comparable intensity to the matrix-isolated band of the ozone monomer, but after 10 minutes its intensity flattens out throughout the irradiation; a similar trend was observed by Dyer et al. (1997). At the later stages of the irradiation, a second shoulder appears on the ν_3 fundamental at 1042 cm^{-1}, which can be attributed to the formation of the [$O_3 \ldots O_3$] van der Waals complex (Bahou et al. 2001).

The temporal evolution of the 1037 cm^{-1} peak is depicted in Figure 4 (*top*), where a value of $A = 1.4 \times 10^{-17}$ molecules cm^{-1} was used (Smith et al. 1985). After the irradiation, the column density is $(1.9 \pm 0.2) \times 10^{16}$ molecules cm^{-2}, where it remains constant throughout the isothermal stage. But upon heating, more ozone begins to form, reaching a maximum at about 38 K of $(3.5 \pm 0.5) \times 10^{16}$ molecules cm^{-2}. At 64 K the oxygen matrix has sublimed completely; no ozone is left.

3.2. *Mass Spectrometry*

The temporal profiles of the signals at $m/e = 32$ and $m/e = 48$ are shown in Figure 4. Note that signal at $m/e = 48$ can originate from two processes: first, the sublimed ozone is ionized in the electron impact ionizer to O_3^+; second, ionized molecular oxygen O_2^+ can undergo ion-molecule reactions with neutral oxygen molecules in the ionizer to form O_3^+. In addition, two channels can contribute to $m/e = 32$: the typical electron impact ionization of molecular oxygen to give O_2^+ and a fragmentation of ionized ozone in the electron impact ionizer to atomic oxygen and ionized molecular oxygen. Most importantly, during the

irradiation process no oxygen or ozone is found to sublime from the solid sample into the gas phase, indicating that sample heating is negligible. As the temperature program is started, weakly bound oxygen molecules possibly from the sample surface begin to sublime from the ice at temperatures between 28 and 43 K (Fig. 4); the oxygen matrix can be seen coming off, where presumably the signal at ∼40 K (∼170 minutes) represents the bulk amorphous oxygen ice, whereas the crystalline phase should be more strongly bound. Finally, the ozone starts subliming at temperatures between 58 and 73 K. The ion current peaks of the subliming oxygen at 38 K and of ozone at 67 K are consistent with those of a previous study, where the sublimation temperatures were determined to be 35 and 63 K for oxygen and ozone, respectively (Fama et al. 2002). Since molecular oxygen and ozone can both result in signal at $m/e = 32$ and 48, it is imperative to actually calculate the true partial pressure of ozone via matrix interval algebra (Kaiser et al. 1995) using electron impact ionization cross sections from Cosby (1993; O_2) and Newson et al. (1995; O_3). The results of this transformation are shown in Figure 5. By integrating this graph and accounting for the effective pumping speed of ozone in our machine (773 liters s^{-1}), we can compute a *lower limit* of the newly formed ozone molecules to be $(2.5 \pm 0.8) \times 10^{16}$ molecules. This is considerably lower, by a factor of 4, than the value determined by the column density obtained from the infrared data. This is due to the well-known fact that the ozone that sublimes from the first stage of the cold head target can actually recondense on the second cold head stage. This effectively increases the pumping speed of ozone and hence mimics a lower ozone partial pressure than the actual current value (Kaiser et al. 1995).

4. DISCUSSION

4.1. *The Dissociation Pathway*

Based on the experimental results, the following formation processes are likely. The infrared spectroscopic detection of ozone and the accompanying [$O_3 \ldots O$] complex verifies that the interaction of the keV electrons with the oxygen molecule must lead to a homolytic bond cleavage, thus forming two oxygen atoms. Cosby (1993) investigated the reaction dynamics of molecular oxygen with ionizing radiation. Upon interaction with

keV electrons, two major reaction pathways are likely to produce atomic oxygen (Cosby 1993). The first,

$$O_2(X\,^3\Sigma_g^-) \rightarrow O(^3P) + O(^3P), \qquad (4)$$
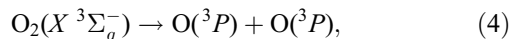
is formally spin-forbidden and requires 498 kJ mol⁻¹ (5.16 eV); the second,

$$O_2(X\,^3\Sigma_g^-) \rightarrow O(^1D) + O(^3P), \qquad (5)$$
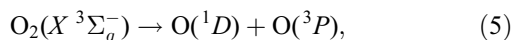
presents a spin-allowed process and requires 688 kJ mol⁻¹ (7.13 eV). Note that half of the atomic oxygen formed via the second process is in its first electronically excited state. However, prior to dissociation by reaction (4), vertical excitation from the $X\,^3\Sigma_g^-$ ground state into one of the repulsive potential energy surfaces, $c\,^1\Sigma_u^-$, $A'\,^3\Delta_u$, or $A\,^3\Sigma_u^+$ states, is suggested; these surfaces actually lie about 6 eV above the ground state, which adiabatically correlates with both ground-state oxygen atoms. The generation of the electronically excited O(¹D) atoms requires excitation into a potential energy surface even higher in energy; Cosby (1993) suggested a dissociation of molecular oxygen from the $B\,^3\Sigma_u^-$ state, where a vertical transition lies about 8 eV above the ground state. It is important to bear in mind that these nascent oxygen atoms released from equations (4) and (5) are born with kinetic energies extending up to 2 eV. There is also some experimental evidence to support the fact that at electron energies above 100 eV reaction (5) becomes the dominant process (Cosby 1993). If we are generating $(3.5 \pm 0.5) \times 10^{16}$ ozone molecules cm⁻², at least an identical number of oxygen atoms are required to react with molecular oxygen to form ozone. Since one oxygen molecule can form two oxygen atoms, $(1.8 \pm 0.3) \times 10^{16}$ molecules of oxygen cm⁻² have to undergo a homolytic bond rupture, i.e., $(5.4 \pm 1.2) \times 10^{16}$ molecules of oxygen over the total sample area. Considering the implantation of 1.5×10^{15} electrons (§ 2), each 5 keV electron cleaves at least 36 ± 6 oxygen molecules. This would result in the formation of 72 ± 13 ozone molecules per implanted electron. Consequently, each electron has to transfer at least 213 ± 40 (reaction [4]) or 285 ± 50 eV (reaction [5]) from its kinetic energy to the oxygen matrix to generate purely ground-state oxygen atoms O(³P) or half of the atomic species in their O(¹D) excited state. This translates to a loss of about 5% of the energy from the incident electron. Therefore, based on the energetics, the formation of the ozone molecule can be accounted for quantitatively.

4.2. *The Actual Reaction Pathway*

The infrared spectroscopic identification of the [O₃...O] complex and of matrix-isolated ozone monomers at 11 K suggests that at low temperatures, at least two nonequilibrium processes involving suprathermal oxygen atoms prevail. As indicated in § 4.1, a homolytic bond rupture of the oxygen molecule yields two oxygen atoms that have an excess kinetic energy of less than 2 eV. Since these species are not in thermal equilibrium with the surrounding matrix, the energetic oxygen atoms are classified as suprathermal or nonequilibrium species. The detection of an [O₃...O] complex could indicate the involvement of two neighboring oxygen molecules (O₂)₂. Here, one of the oxygen molecules is cleaved homolytically to form initially an [O₂...O...O] complex. If the released oxygen atoms have sufficient excess energy to overcome the diffusion barrier in the matrix, they can escape the [O₂...O...O] complex and can react with a molecule
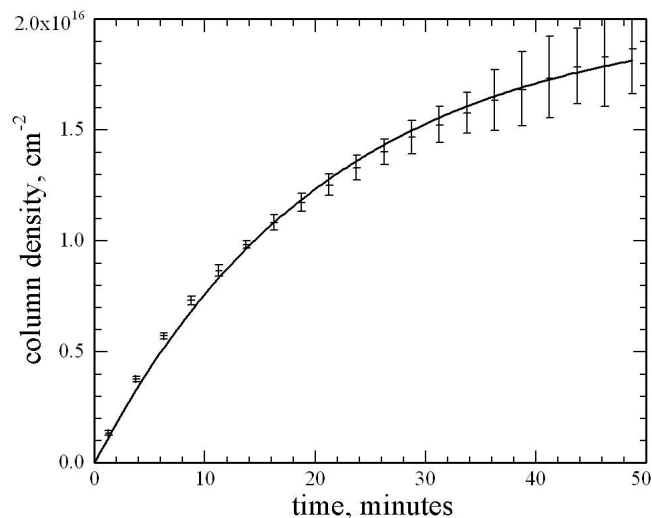
Fig. 6.—Fit of the ozone column density according to eq. (7).

in the matrix at a site distant from the initial complex to form ozone via

$$O_2(X\,^3\Sigma_g^-) + O(^3P) \rightarrow O_3(X\,^1A_1). \qquad (6)$$
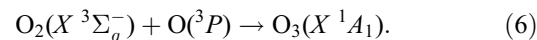
However, those oxygen atoms born without sufficient excess energy cannot escape from the initial complex; the oxygen atom rather reacts without barrier with a *neighboring* oxygen molecule within the matrix cage at 11 K (also forming ozone by reaction [6]). If, however, the remaining oxygen atom does not possess enough kinetic energy to escape, an [O₃...O] complex will remain in the oxygen matrix, as observed.

Postulating the involvement of *neighboring* oxygen molecules (O₂)₂ and assuming that reactions (4) and (5) proceed much faster than reaction (6), the formation of ozone at 11 K should follow pseudo–first-order kinetics during the irradiation process. As a matter of fact, we were able to fit the temporal evolution of the ozone column density, [O₃](t), via pseudo–first-order kinetics using

$$[O_3](t) = a\bigl(1 - e^{-kt}\bigr). \qquad (7)$$

Figure 6 depicts the best fit of the ozone profile with $a = (2.0 \pm 0.1) \times 10^{16}$ molecules cm⁻² and $k = (7.9 \pm 0.3) \times 10^{-4}$ s⁻¹. These values compare well to those of experiments carried out with UV photolysis, where Schriver-Mazzuoli et al. (1995) determined a value of $k = 1.0 \times 10^{-3}$ s⁻¹, and a value of $k = 7.8 \times 10^{-3}$ s⁻¹ (estimated) from Gerakines et al. (1996) after irradiation with a medium-pressure mercury discharge lamp ($\Phi \sim 10^{15}$ photons cm⁻² s⁻¹ with $E_{h\nu} > 6$ eV). The rate cannot be compared to experiments using keV ion bombardment, as the authors did not present an analytical solution of the temporal evolution of ozone (Baragiola et al. 1999). However, recall that in our experiment we have identified a third reaction mechanism during heating of the ice to 38 K. The increasing column density of ozone is an explicit indication that even after the irradiation has stopped, the oxygen matrix still stores oxygen atoms at 11 K. When the electron irradiation stops, the production of excited oxygen atoms ceases, as well. In the gas phase, O(¹D) has a lifetime of about 110 s (Bhardwaj & Haider 2002); in the solid state the lifetime is expected to be on the order of a few hundred milliseconds (Mohammed 1990), and after a 3600 s equilibration time at 11 K, all excited oxygen

atoms have relaxed to their ^3P ground state. The question still remains as to why upon heating a second pathway to ozone formation exists—generating almost the same amount of ozone as was generated during irradiation. As indicated earlier, the formation of ozone is the result of an oxygen atom colliding with an oxygen molecule. However, steric effects dictate that not all oxygen atoms released react with the oxygen molecule to form ozone (Levine 2005). Oxygen atoms failing to enter the cone of acceptance of the oxygen molecule do not react and hence can be stored in the matrix at 11 K. At 38 K, which translates to about 0.003 eV, the oxygen atoms might be able to overcome the diffusion barrier and collide with a neighboring oxygen molecule in the correct geometric orientation.

4.3. *The Cyclic Ozone Molecule*

Besides the bent C_{2v} symmetric structure, electronic structure calculations predict that a second isomer of ozone should also exist (Xantheas et al. 1991; Hernández-Lamoneda et al. 2002; Siebert et al. 2002). A cyclic isomer holding D_{3h} symmetry was suggested to be 1.34 eV less stable than the bent ozone molecule. Once the bent C_{2v} structure has been formed, the barrier to isomerization to the D_{3h} isomer is calculated to be 2.37 eV; however, the dissociation energy of the bent ozone (1.05 eV) lies below the energy of the D_{3h} structure. Therefore, even if an ozone molecule formed in the 11 K matrix interacts with a second electron via an inelastic energy transfer, the dissociation to atomic plus molecular oxygen is more likely than its isomerization to cyclic ozone. In addition, the preferred channel for atomic oxygen reaction with an oxygen molecule in the solid is by addition to one of the oxygen atoms to form the C_{2v} structure. This atom-radical reaction does not have an entrance barrier. In comparison, the entrance barrier to the D_{3h} structure is estimated to be at least 2 eV (Xantheas et al. 1991), which is higher than the predicted translational energy of the suprathermal atoms generated in reactions (4) and (5). As a matter of fact, the distribution maxima of the translational energies of $O(^3P)$ and $O(^1D)$ were predicted to be 0.5 and 1.7 eV, respectively (Cosby 1993). This can explain why the cyclic ozone molecule was not observed.

5. ASTROPHYSICAL IMPLICATIONS

We have demonstrated that when condensed molecular oxygen is subjected to irradiation from energetic electrons, the formation of ozone can be fit by pseudo–first-order kinetics. A similar process is expected to occur within the apolar ice grains of interstellar clouds via elastic energy transfer processes from the release of energetic electrons in the track of Galactic cosmic-ray particles—a process that has been shown to account for 99.9% of the energy transfer processes from energetic cosmic-ray particles interacting with low-temperature ices (Kaiser & Roessler 1998). Most importantly, molecular oxygen itself need not be a major constituent of an ice for ozone to be generated; in fact, any oxygen-bearing species can potentially act as a precursor to form oxygen atoms via electronic and nuclear interaction processes of the cosmic-ray particle with the ices. An example is the irradiation of carbon dioxide, which has already been shown to generate ozone (Bennett et al. 2004). Here, the temporal evolution of ozone could be fit with a consecutive reaction scheme. The first reaction would be the recombination of two oxygen atoms within the matrix by

$$O(^3P) + O(^3P) \rightarrow O_2(X\,^3\Sigma_g^-), \qquad (8)$$
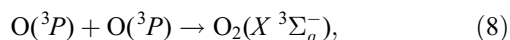
followed by the addition of a third oxygen atom to generate ozone as given in reaction (6). However, in this case we must also con-
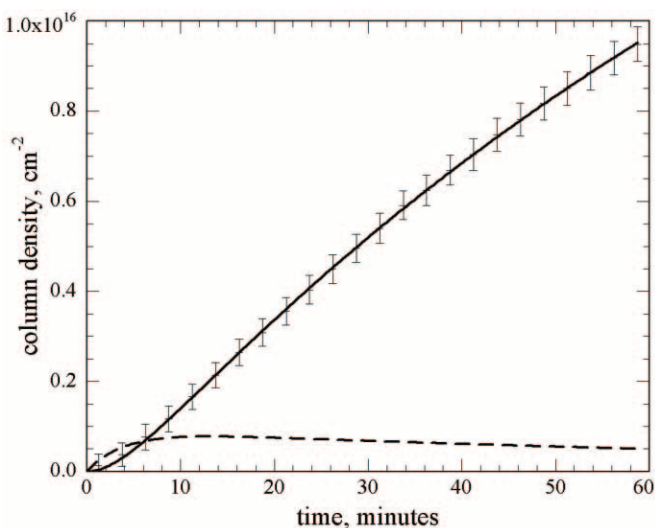
Fig. 7.—Fit of ozone (*solid line*) and inferred molecular oxygen (*dashed line*) column densities according to eqs. (10) and (9), respectively, after carbon dioxide ice was subjected to 5 keV electrons at 0.1 μA for 60 minutes (data from Bennett et al. 2004).

sider the formation of the oxygen molecule itself. Here we were able to fit the data using the consecutive (A → B → C) reaction scheme, where we formally consider A as a carbon dioxide trimer, $[(CO_2)_3]$, in the matrix. Upon irradiation, the latter decomposes to a complex B, $[(CO)_3...O...O_2]$ or $[(CO)_2...(CO_2)...O_2]$, where two oxygen atoms have already combined to form molecular oxygen via equation (8) within the matrix cage of the complex, and finally the third oxygen atom combines to form ozone by reaction (6) to form a formal complex C, $[(CO)_3...O_3]$. Thus, the temporal evolution of the oxygen and ozone species column densities can be fit using the following two-step consecutive pseudo–first-order kinetics (Steinfeld et al. 1999, p. 26):

$$[O_2](t) = \frac{k_1 b}{k_2 - k_1}\left(e^{-k_1 t} - e^{-k_2 t}\right), \qquad (9)$$

$$[O_3](t) = b\left(1 - \frac{k_2}{k_2 - k_1}e^{-k_1 t} + \frac{k_1}{k_2 - k_1}e^{-k_2 t}\right), \quad (10)$$

where k_1 represents the reaction rate of reaction (8) and k_2 is the rate of reaction (6). Figure 7 represents the best fit of the ozone profile from a carbon dioxide ice, where $b = (2.2 \pm 0.1) \times 10^{16}$ molecules cm^{-2}, $k_1 = (1.7 \pm 0.1) \times 10^{-4}$ s^{-1}, and $k_2 = (4.3 \pm 0.2) \times 10^{-3}$ s^{-1}. By investigating the reaction mechanisms, we are able to extract additional information about intermediates we cannot observe in our experiment, in this case the case of oxygen formation within the carbon dioxide matrix (Fig. 7). We can investigate the relative rates of k_1 and k_2. Once oxygen molecules are formed, they can quickly react to form ozone; consequently, it might be possible to observe ozone within solar system ices, even though molecular oxygen itself is undetectable. These results may help to explain why model simulations of ozone within the Martian atmosphere fail to be able to reproduce the observed column densities, as these models are based only on gas-phase photochemical reactions (Lefèvre et al. 2004), whereas it is well known that carbon dioxide ices are present and therefore subject to irradiation on the planet's surface (Litvak et al. 2004). It is well known that molecular oxygen is a product from experiments studying the effects of irradiation of water (Orlando & Sieger 2003; Zheng et al. 2006). However,

ozone has not yet been observed in these systems, perhaps because oxygen atoms cannot diffuse through a matrix, indicating that neighboring oxygen molecules may be required to generate oxygen, which may not be sufficiently abundant within pure water ices—conversely, hydrogen atoms can diffuse through the matrix, making additional reactions with molecular oxygen possible, which may also impede ozone formation. It is also interesting to note the possible relevance of the additional thermal pathway observed in the present experiments, which may be of some relevance to the Jovian satellites, where localized tidal heating effects could prompt the formation of ozone from trapped molecular and atomic oxygen species within the ice. Thus, it is evident that in order to elucidate the formation of ozone within the more diverse chemical compositions and temperatures of our solar system, further studies need to be carried out that emphasize how such effects could change the formation rates and pathways to form ozone.

REFERENCES

Adler-Golden, S. M., Langhoff, S. R., Bauschlicher, C. W., Jr., & Carney, G. S. 1985, J. Chem. Phys., 83, 255

Angel, J. R., Cheng, A. Y. S., & Woolf, N. J. 1986, Nature, 322, 341

Bahou, M., Schriver-Mazzuoli, L., & Schriver, A. 2001, J. Chem. Phys., 114, 4045

Baragiola, R. A., Atteberry, C. L., Bahr, D. A., & Jakas, M. M. 1999, Nucl. Instrum. Methods Phys. Res. B, 157, 233

Barth, C. A., Hord, C. W., & Stewart, A. I. 1973, Science, 179, 795

Beichman, C. A., Woolf, N. J., & Lindensmith, C. A., eds. 1999, The *Terrestrial Planet Finder* (*TPF*): A NASA Origins Program to Search for Habitable Planets (Pasadena: JPL)

Bennett, C. J., Jamieson, C., Mebel, A. M., & Kaiser, R. I. 2004, Phys. Chem. Chem. Phys., 6, 735

Bhardwaj, A., & Haider, S. A. 2002, Adv. Space Res., 29, 745

Brewer, L., & Wang, L.-F. 1972, J. Chem. Phys., 36, 759

Cairns, B. R., & Pimentel, G. C. 1965, J. Chem. Phys., 43, 3432

Calvin, W. M., & Spencer, J. R. 1997, Icarus, 130, 505

Chaabouni, H., Schriver-Mazzuoli, L., & Schriver, A. 2000, J. Phys. Chem. A, 104, 6962

Chapman, S. 1930, Mem. R. Meteorol. Soc., 3(26), 103

Cooper, J. F., Johnson, R. E., Mauk, B. H., Garrett, H. B., & Gehrels, N. 2001, Icarus, 149, 133

Cosby, P. C. 1993, J. Chem. Phys., 98, 9560

Crowley, J. N., & Sodeau, J. R. 1989, J. Phys. Chem., 93, 3100

Dyer, M. J., Bressler, C. G., & Copeland, R. A. 1997, Chem. Phys. Lett., 266, 548

Ehrenfreund, P., Breukers, R., d'Hendecourt, L., & Greenberg, J. M. 1992, A&A, 260, 431

Fama, M., Bahr, D. A., Teolis, B. D., & Baragiola, R. A. 2002, Nucl. Instrum. Methods Phys. Res. B, 193, 775

Freiman, Yu. A., & Jodl, H. J. 2004, Phys. Rep., 401, 1

Gerakines, P. A., Schutte, W. A., & Ehrenfreund, P. 1996, A&A, 312, 289

Greenberg, J. M. 1984, Sci. Am., 250, 124

Hall, D. T., Feldman, P. D., McGrath, M. A., & Strobel, D. F. 1998, ApJ, 499, 475

Hartley, W. N. 1881, J. Chem. Soc., 39, 111

Hernández-Lamoneda, R., Salazar, M. R., & Pack, R. T. 2002, Chem. Phys. Lett., 355, 478

Johnson, R. E. 1990, Energetic Charged Particle Interactions with Atmospheres and Surfaces (Berlin: Springer)

Johnson, R. E., & Jesser, W. A. 1997, ApJ, 480, L79

Jones, L. H., Agnew, S. F., Swanson, B. I., & Ekberg, S. A. 1986, J. Chem. Phys., 85, 428

Jones, L. H., Swanson, B. I., Agnew, S. F., & Ekberg, S. A. 1985, J. Phys. Chem., 89, 2982

Kaiser, R. I., Jansen, P., Peterson, K., & Roessler, K. 1995, Rev. Sci. Instrum., 66, 5226

Kaiser, R. I., & Roessler, K. 1998, ApJ, 503, 959

Kasting, J. F., & Catling, D. 2003, ARA&A, 41, 429

Lacombe, S., Cemic, F., Jacobi, K., Hedhili, M. N., Le Cont, Y., Azria, R., & Tronc, M. 1997, Phys. Rev. Lett., 79, 1146

Lefèvre, F., Lebonnois, S., Montmessin, F., & Forget, F. 2004, J. Geophys. Res., 109, E07004

Léger, A. 2000, Adv. Space Res., 25, 2209

Levine, R. D. 2005, Molecular Reaction Dynamics (Cambridge: Cambridge Univ. Press)

Litvak, M. L., et al. 2004, Sol. Syst. Res., 38, 167

Mathis, J. S., Mezger, P., & Panagia, N. 1983, A&A, 128, 212

Mohammed, H. H. 1990, J. Chem. Phys., 93, 412

Newson, K. A., Luc, S. M., Price, S. D., & Mason, N. J. 1995, Int. J. Mass Spectrom. Ion Processes, 148, 203

Noll, K. S., Johnson, R. E., Lane, A. L., Domingue, H. A., & Weaver, H. A. 1996, Science, 273, 341

Noll, K. S., Roush, D. P., Cruikshank, D. P., Johnson, R. E., & Pendleton, Y. J. 1997, Nature, 388, 45

Okabe, M. 1978, Photochemistry of Small Molecules (New York: Wiley)

Orlando, T. M., & Sieger, M. T. 2003, Surface Sci., 528, 1

Owen, T. 1980, in Strategies for the Search for Life in the Universe, ed. M. D. Papagiannis (Dordrecht: Reidel), 177

Schriver-Mazzuoli, L., de Saxcé, A., Lugez, C., Camy-Peyret, C., & Schriver, A. 1995, J. Chem. Phys., 102, 690

Selsis, F., Despois, D., & Parisot, J.-P. 2002, A&A, 388, 985

Siebert, R., Fleurat-Lessard, P., Schinke, R., Bittereová, M., & Farantos, S. C. 2002, J. Chem. Phys., 116, 9749

Siebert, R., & Schinke, R. 2003, J. Chem. Phys., 119, 3092

Smith, M. A. H., Rinsland, C. P., Fridovich, B., & Rao, K. N. 1985, in Molecular Spectroscopy—Modern Research, Vol. 3, ed. K. N. Rao (London: Academic), 111

Spencer, J. R., & Calvin, W. M. 2002, AJ, 124, 3400

Spencer, J. R., Calvin, W. M., & Person, M. J. 1995, J. Geophys. Res., 100, 19049

Steinfeld, J. I., Francisco, J. S., & Hase, W. L. 1999, Chemical Kinetics and Dynamics (2nd ed.; Upper Saddle River: Prentice Hall)

Strazzulla, G., & Johnson, R. E. 1991, in Comets in the Post-Halley Era, ed. R. L. Newburn, Jr., M. Neugebauer, & J. Rahe (Dordrecht: Kluwer), 243

Thomas, R. 1993, Gene, 135, 77

Tielens, A. G. G. M., & Hagen, W. 1982, A&A, 114, 245

Vandenbussche, B., et al. 1999, A&A, 346, L57

Vidal, R. A., Bahr, D., Baragiola, R. A., & Peters, M. 1997, Science, 276, 1839

Xantheas, S. S., Atchity, G. J., Elbert, S. T., & Ruedenberg, K. 1991, J. Chem. Phys., 94, 8054

Zheng, W.-J., Jewitt, D., & Kaiser, R. I. 2006, ApJ, in press